# Exposing the role of pre-association in interfacial proton-coupled electron transfer

Noah B. Lewis,[i] Joel G. Gardner,[i] Neil K. Razdan,[i] Shane Ardo,[ii,iii,iv] and Yogesh Surendranath[i,v]*

i) Department of Chemistry, Massachusetts Institute of Technology, Cambridge, MA 02139, USA

ii) Department of Chemistry, University of California Irvine, Irvine, CA 92976, USA

iii) Department of Chemical and Biomolecular Engineering, University of California Irvine, Irvine, CA 92976, USA

iv) Department of Materials Science and Engineering, University of California Irvine, Irvine, CA 92976, USA

v) Department of Chemical Engineering, Massachusetts Institute of Technology, Cambridge, MA 02139, USA

* Corresponding author: yogi@mit.edu

## Abstract

Interfacial proton-coupled electron transfer (I-PCET) reactions are typically viewed as single elementary reaction steps even though analogous solution-phase reactivity is known to require pre-association of proton donor and acceptor. Herein, we examine the role of pre-association in I-PCET to a molecularly well-defined graphite-conjugated carboxylic acid (GC-COOH) surface site. We quantify electrolyte proton activity and I-PCET kinetics in acidic, acetate buffered, and alkaline electrolytes as a function of $NaClO_4$ concentration, ranging from 1 mole $kg^{-1}$ to 17 mole $kg^{-1}$. Upon accounting for the previously measured proton activity dependence of I-PCET kinetics to GC-COOH, we find that rate of I-PCET is systematically attenuated by factors of 4.3 and 4.6 over this range of $NaClO_4$ concentration in acidic and acetate buffered media, respectively. In contrast, the rate of I-PCET remains unchanged within error across $NaClO_4$ concentration in alkaline electrolyte. Based on these observations, we propose a multiple-step model for I-PCET in acidic media that invokes quasi-equilibrated displacement of $Na^+$ from the interface to form hydrogen-bonded pre-association complexes prior to rate-limiting concerted proton-electron transfer. Increased $NaClO_4$ concentration is invoked to increase $Na^+$ activity in the bulk vs the interface, inhibiting pre-association complex formation and the overall I-PCET rate. These studies emphasize the non-innocent role of support electrolyte species and expose the key role of pre-association equilibria in I-PCET mechanisms. The work also suggests that control over pre-association equilibria could be used as an additional handle for tailoring the kinetics of interfacial ion transfer reactions.

## Introduction

Interfacial proton-coupled electron transfer (interfacial PCET or I-PCET) reactions play a central role in electrochemical catalysis and energy conversion technologies.[1–4] I-PCET reactions involve the reductive formation or oxidative scission of surface-hydrogen bonds and are thus key elementary reaction steps in hydrogen evolution and oxidation,[5,6] oxygen evolution and reduction,[7,8] carbon dioxide and nitrogen reduction,[9,10] and fuel oxidation.[8,11] Beyond electrocatalysis, I-PCET is operative in the stoichiometric reactions that occur in supercapacitors[12,13] and sensors[14,15] as well as non-Faradaic

catalysis.[16–19] In many instances, I-PCET is deleterious, including in corrosion,[2] parasitic hydrogen evolution,[10,20,21] and electrolyte breakdown in both aqueous[22] and aprotic electrolytes.[23–25] Consequently, a deep fundamental understanding of I-PCET reaction mechanisms is critical for the systematic development of sustainable catalysis and chemical energy conversion technologies.

Despite their ubiquity, I-PCET reactions remain poorly understood at a molecular level, particularly in comparison to the rich understanding of electrochemically-driven outer-sphere PCET (OS-PCET) reactions involving soluble molecules. This is in large part due to the distinct reaction mechanisms at play in interfacial as compared to outer-sphere PCET. For OS-PCET, electrons tunnel across the electrochemical double layer (EDL) to oxidize or reduce a soluble molecule and drive proton transfer. Since electrons can tunnel over length scales on par with or greater than the width of the EDL, the ionic composition and structure of the EDL plays a negligible role in OS-PCET kinetics. In contrast, for I-PCET, protons must transit the EDL to bind to specific surface sites and thus the ionic composition and structure of the EDL is expected to play a pronounced role in I-PCET.[26–28]

The foregoing distinction is particularly poignant because of the inherently concerted nature of I-PCET reactions. Electrochemical OS-PCET reactions can proceed via either stepwise pathways with proton transfer either preceding ($PT_1ET_2$) or following ($ET_1PT_2$) a distinct electron transfer step or through a concerted proton-electron transfer (CPET) reaction pathway. In contrast, since electron re-distribution in a metal is nominally barrierless, I-PCET reactions proceed via concerted CPET pathways exclusively. Extensive studies of molecular PCET reactions in solution have shown that CPET pathways proceed through a three-step sequence, involving quasi-equilibrated formation of a hydrogen-bonded pre-association complex between the redox active species and the proton acceptor, rate-limiting CPET, and subsequent dissociation of the successor complex (**Figure 1a**).[29–31] Consequently, it has been shown that the overall rate of CPET is a function of the rate constant for the CPET step and the equilibrium constant for forming the pre-association complex.[30,32,33] Indeed, it has been found that inhibited formation of the pre-association complex can substantially attenuate CPET rates. Despite this rich appreciation of the multi-step nature of CPET reactions between molecules in solution, I-PCET reactions are generally described and modeled as single elementary reaction steps (**Figure 1b**), without explicit consideration of pre-association equilibria or their impact on reaction kinetics. Given the ubiquitous necessity for pre-association in molecular CPET, the obligate concerted nature of I-PCET, and the well-documented proton donor dependence of I-PCET processes,[5,34–37] we hypothesized that similar pre-association equilibria may play a key, but overlooked, role in gating PCET at interfaces (**Figure 1c**). Unfortunately, the inherent complexity of most heterogeneous catalysts makes it difficult to isolate the impact of pre-association from other convoluting factors (e.g. surface restructuring, site blocking, etc.) that may lead to promotion or inhibition of I-PCET.

Previously, we investigated the kinetics of aqueous I-PCET to well-defined reaction sites of graphite-conjugated carboxylic acid electrodes (GC-COOH).[38–40] These materials, which are synthesized through a condensation reaction that links 3,4-diaminobenzoic acid to the native *ortho*-quinone moieties of glassy carbon, display well-resolved voltametric waves corresponding to I-PCET. The resultant pyrazine linkage connects the carboxylate through a continuous π-electron system to the electrode's band states, making it an authentic and molecularly defined host for I-PCET.[38,40–42] Given the facile nature of electron redistribution in the graphitic carbon, the proton transfer coordinate is expected to define the majority of the barrier for I-PCET. Yet, we found that the maximal rate constants for I-PCET to GC-COOH in aqueous media of 20,000 $s^{-1}$ at pH 0, far below the near diffusion limited rate (> $10^9$ $s^{-1}$) of proton exchange between oxo-acids in bulk water.[43,44] This dramatic mismatch implies that the presence of the EDL serves to profoundly attenuate I-PCET rates. We hypothesized that this attenuation may arise in part due to the inhibited formation of the pre-association complex from which interfacial CPET occurs. Since the EDL is

predominantly composed of the inert supporting electrolyte ions in the medium, we envision that changes to the supporting electrolyte strength could report on the dynamics within the EDL required for I-PCET.

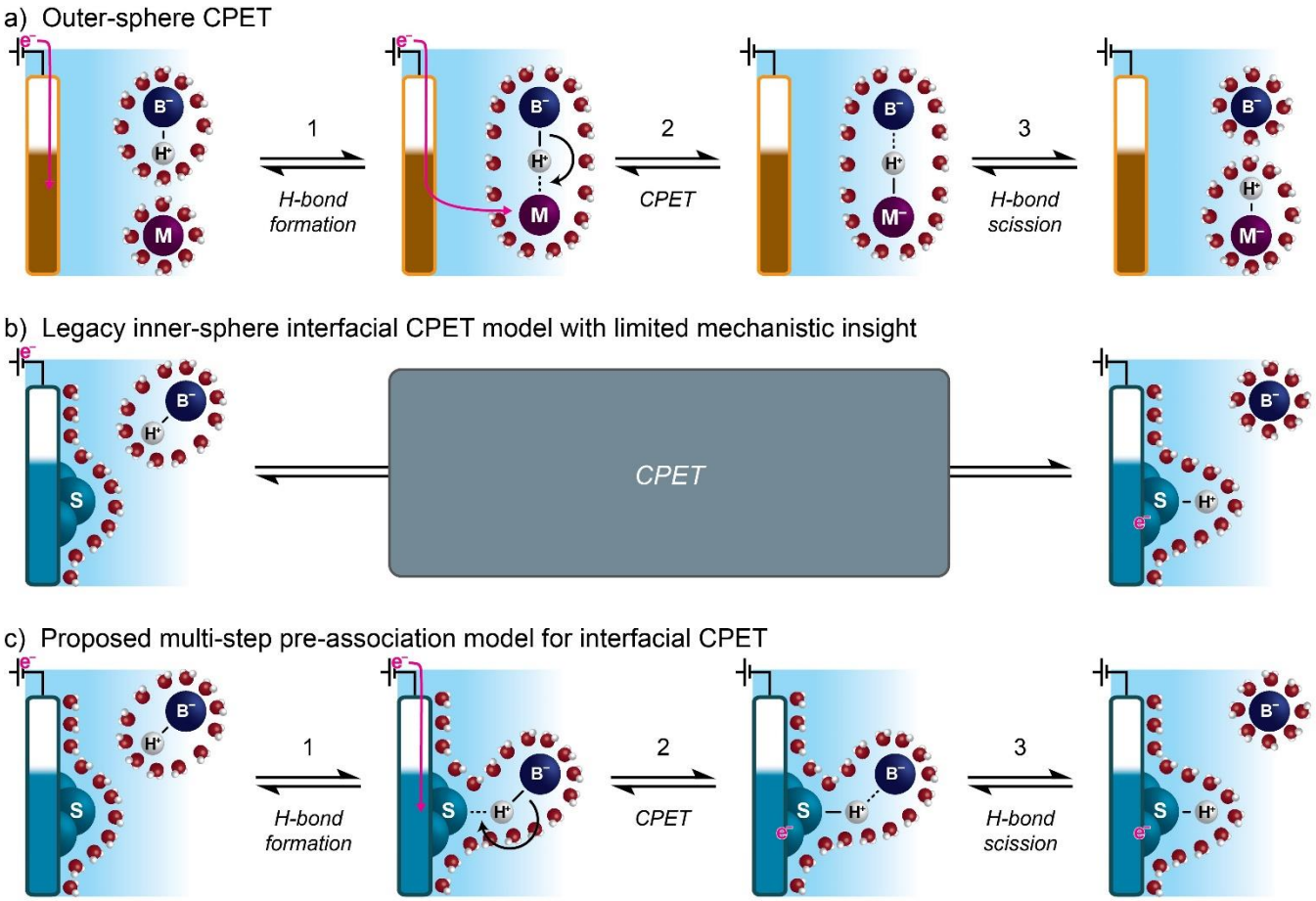


**Figure 1 | Proposed pre-association mechanisms for outer-sphere and interfacial concerted proton-electron transfer (CPET): a)** Outer-sphere CPET occurs in three steps: 1) association of a proton-donating acid "$B^{-}$-$H^{+}$" and a PCET active molecule "M" into a co-solvated hydrogen bonded pre-association complex in solution. 2) Proton transfer from "$B^{-}$" to "M" within the pre-association complex occurs at the same time as electron tunneling from the electrode to "M", forming the PCET-product "$M^{-}$-$H^{+}$". 3) Fragmentation of the successor complex into independently solvated base "$B^{-}$" and PCET product. **b)** Representation of the legacy model for I-PCET that invokes a single elementary step. **c)** Proposed pre-association mechanism for interfacial PCET occurs similarly with 1) Formation of a co-solvated solution acid "$B^{-}$-$H^{+}$" and surface active site "S" pre-association complex at the electrode/electrolyte interface 2) Proton transfer from $B^{-}$" to "M" within the pre-association complex occurs as an electron transfers from the external circuit into the delocalized electrode band states, forming the PCET-product "S-$H^{+}$". 3) Breakage of the successor complex into independently solvated base "$B^{-}$" and protonated surface site.

To investigate the role of the EDL and pre-association on I-PCET mechanisms we measured the thermodynamics and kinetics of I-PCET at GC-COOH electrodes across a wide range of supporting electrolyte concentrations. Specifically, we measure i) proton activity, ii) I-PCET thermochemistry, and iii) I-PCET kinetics in highly acidic, highly alkaline, and buffered electrolytes each containing 1 to 17 molal (moles $kg^{-1}$ or "m") $NaClO_4$. Using a reversible hydrogen electrode to quantify changes in proton

activity across ionic strength, we find that increasing ionic strength increases the proton activity of the acidic electrolyte significantly but the buffered and alkaline electrolytes only minimally. Correspondingly, we also observe the electrode potential of I-PCET at GC-COOH to track largely with ionic-strength-dependent proton activity. Accounting for proton activity changes, we find that I-PCET rates are substantially attenuated in acidic and buffered electrolytes (a decrease in ~0.04 log units per molal, spanning a factor of ~4.5 across the range studied) but largely invariant in basic electrolyte. Based on these findings we develop a mechanistic model for I-PCET that invokes a pre-association step involving exchange of a supporting electrolyte ion with the proton donor/acceptor, prior to rate-limiting CPET. Though classically considered inert, these observations imply that supporting electrolyte, while necessary to establish the EDL potential drop and provide ionic conductivity, nonetheless serves to inhibit pre-association and corresponding I-PCET rates. These findings highlight the critical role of supporting electrolyte ions in modulating interfacial charge transfer kinetics and establishes a framework for understanding how electrolytes influence the kinetics of the I-PCET reactions that underpin electrochemical energy conversion and catalysis.

# Results and Discussion

## Experimental conditions

The studies described below employed $NaClO_4$ based aqueous electrolytes due both to sodium perchlorate's relative inertness and its technological applicability. Unlike other commonly used highly soluble electrolytes, degassed aqueous $NaClO_4$ is not expected to contribute to a solid electrolyte interphase (SEI) that could potentially convolute kinetic analysis of I-PCET.[45–51] Furthermore, highly concentrated $NaClO_4$-based "Water in Salt" Electrolytes (WiSE), being far more economical than lithium bis(trifluoromethane)sulfonimide and analogous electrolytes and maintaining a wide electrochemical window and high conductivity,[13,52–56] are practically relevant to a number of catalytic[57] and energy storage technologies.

All data in this study were collected under three proton donor/acceptor conditions (unbuffered acidic, buffered near-neutral, and unbuffered alkaline) each for 1 m, 5 m, 9 m, 13 m, and 17 m $NaClO_4$ allowing for comparisons between acidity conditions and across a wide range of ionic strength. We assessed I-PCET across this extreme range of solution concentrations to perturb reaction conditions significantly enough to elicit the hypothesized ionic strength-dependent ion transfer reactivity. All measurements were conducted in solutions with consistent proton donor and acceptor ratios at concentrations not easily altered under the experimental conditions. To do so, the proper amount of $HClO_4$, NaOH, or acetic acid/sodium acetate buffer was added such that in the absence of dry $NaClO_4$ the electrolytes would contain a consistent relative mole fraction equivalent to 0.1 M $HClO_4$ for the acidic media, 0.1 M NaOH for the basic media, and 0.05 M acetic acid (AcOH) plus 0.05 M sodium acetate (NaOAc) for the buffered media. These donor/acceptor concentrations were chosen to minimize pH changes during and between experiments while having minimal effect on the overall concentration of dissolved species.

## Effect of ionic-strength on proton activity at a reversible hydrogen electrode

Before assessing the effect of electrolyte concentration on I-PCET thermodynamics and kinetics at GC-COOH it was first essential to quantify how ionic strength affects the activity of I-PCET reactants in concentrated aqueous media. Given that highly concentrated solutions are observed to be more acidic,[58] it is essential to differentiate if kinetic changes in I-PCET reactivity are simply due to a shift in

donor/acceptor equilibria or to additional concentration-dependent processes. As such, it is imperative to understand how the relative proton donor and proton acceptor *activities* are affected by a change in ionic strength for a fixed ratio of proton donor and acceptor molar *concentrations*.

To determine the electrochemical proton activity of each electrolyte, we measured the potential of a reversible hydrogen electrode (RHE) comprised of a platinum on PTFE gas diffusion electrode (Pt-GDE) under 1 atm $H_2$. This method was necessary given the limitations of using a standard pH meter in concentrated media.[3,58] An RHE measures the potential set by the interchange between solution protons and $H_2$ gas, which is the equilibrium set by the hydrogen evolution reaction (HER) and the hydrogen oxidation reaction (HOR). In acidic media, where $H_3O^+$ is the proton donor and water is the proton acceptor, the HER/HOR equilibrium can be written as:

$$2\ H_3O^+ + 2\ e^- \overset{E_{RHE}}{\rightleftharpoons} H_2 + 2\ H_2O \qquad \textbf{Reaction 1}$$

And in alkaline conditions where water is the proton donor and $OH^-$ is the proton acceptor:

$$2\ H_2O + 2\ e^- \overset{E_{RHE}}{\rightleftharpoons} H_2 + 2\ OH^- \qquad \textbf{Reaction 2}$$

The electrode potential of this equilibrium ($E_{RHE}$) can be defined in reference to $H_3O^+$ activity for **Reaction 1** through the Nernst equation as:

$$E_{RHE} = E_{SHE} - \frac{RT}{2F}\ln\left(\frac{(a_{H_2O})^2 \times P_{H_2}}{(a_{H_3O^+})^2}\right) \qquad \textbf{Equation 1}$$

$E_{RHE}$ can also be referenced to $OH^-$ activity:

$$E_{RHE} = E_{SHE} - \frac{RT}{2F}\ln\left(\frac{(a_{OH^-})^2 \times P_{H_2}}{(a_{H_2O})^2} \times \frac{1}{K_w{}^2}\right) \qquad \textbf{Equation 2}$$

Where $E_{SHE}$ is the potential of the standard hydrogen electrode (SHE) benchmarked as 0 V; *R, T*, and *F* are the gas constant, temperature, and the Faraday constant, respectively; $a_{H_3O^+}$, $a_{H_2O}$, and $a_{OH^-}$ are the chemical activities of the subscripted species; $P_{H_2}$ is the partial pressure of $H_2$ gas; and $K_w$ is the auto-dissociation constant of water. At a constant $P_{H_2}$ and T, $E_{RHE}$ is therefore a direct reporter of the electrochemical activity of protons, or effective pH ($pH_{eff}$) of the medium:

$$pH_{eff} = -\log\left(\frac{a_{H_3O^+}}{a_{H_2O}}\right) = -\log\left(\frac{a_{H_2O}}{a_{OH^-}} \times K_w\right) \qquad \textbf{Equation 3}$$

Where at room temperature:

$$E_{RHE} = -0.059\ V \times pH_{eff} \qquad \textbf{Equation 4}$$

The relative proton activity of the system is exactly analogous to the ratio of the activities of the proton donor and acceptor species relevant in I-PCET. Importantly, casting the RHE reactions in this way acknowledges the identity and role of all proton donor/acceptor species, including water whose ionic-strength-dependent activity is frequently neglected.[57,59]

For electrolytes of three different well-defined proton donor/acceptor concentrations we observed markedly different effects on $E_{RHE}$ as a function of electrolyte ionic strength. **Figure 2** displays the $E_{RHE}$ of a Pt-GDE from solutions of 1 m to 17 m $NaClO_4$ with added 0.1 M $HClO_4$, 0.1 M acetate buffer, and 0.1 M NaOH. In the presence of 1 m $NaClO_4$, $E_{RHE}$ equals −0.055 V vs SHE for the acidic electrolyte, –0.254 V vs SHE for the buffered electrolyte, and –0.742 V vs SHE for the alkaline electrolyte. These measured $E_{RHE}$ values relay proton activities equivalent to pH 0.9, pH 4.3, and pH 12.6 respectively. Using a pH probe, the respective pH values of these 1 m $NaClO_4$ solutions were found to be 1.0, 4.3, and 12.6, indicating close agreement of these two methods at this relatively dilute concentration. Moving to higher concentrations, different trends were observed for the acidic, buffered, and alkaline media. From 1 m to 17 m, $E_{RHE}$ for the acidic electrolytes shifted positively to +0.056 V vs SHE (red). Over the same range, $E_{RHE}$ for the buffered electrolyte and alkaline electrolytes shifted negatively to −0.271 V vs SHE (green) and −0.767 V vs SHE (blue), respectively. Linear regression (gray dotted lines) of $E_{RHE}$ values from 1 m to 17 m return +6.9 ± 0.6 mV $m^{-1}$, −1.1 mV $m^{-1}$ ± 0.5 mV $m^{-1}$, and −1.7 mV $m^{-1}$ ± 0.4 mV $m^{-1}$ slopes for the acidic, buffered, and basic electrolytes respectively (± error equals 2σ). While a measured change in $E_{RHE}$ might in principle be convoluted by artifacts of liquid junction potentials,[58] we estimate that these contributions are small (see **Supplementary Note 1**) and the measured change thus arises predominantly from changes in activity. The increase of $E_{RHE}$ in the $HClO_4$ electrolytes indicates an increase in the activity of the proton donor, $H_3O^+$, versus the proton acceptor, $H_2O$. From **Equation 1**, this pH change is equivalent to a 1.9 unit drop in $pH_{eff}$. Conversely, a negative shift of $E_{RHE}$ in the buffered and alkaline electrolytes relay a slight *increase* in $pH_{eff}$ of about 0.27 and 0.41 units for the buffered and alkaline electrolytes, respectively. As a function of molality, a negative $E_{RHE}$ shift corresponds to an increase in proton acceptor activity relative to proton donor activity, i.e. acetate versus acetic acid and hydroxide versus water. These data demonstrate that in the presence of a common electrolyte ($NaClO_4$), the ionic-strength-dependent proton activity of the three donor/acceptor conditions at constant molar ratio vary widely depending on the identity of the donors and acceptors involved.

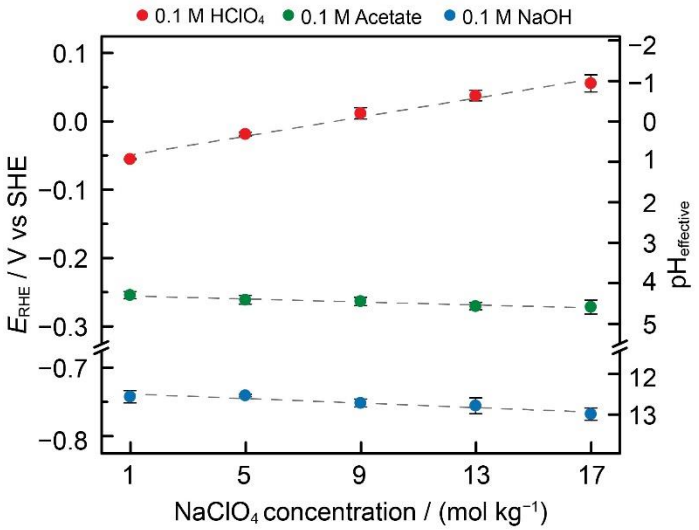


**Figure 2 | $E_{RHE}$ as a function of molality.** Potentials are of a Pt-GDE with the solution proton activity set by 0.1 M $HClO_4$ (red), acetate buffer (green), and NaOH (blue). Points are means of three measurements, error bars represent 2σ, and dotted gray lines represent linear regressions of each data set. On the right vertical axis $E_{RHE}$ is converted to effective pH by dividing the $E_{RHE}$ values of the left axis by 0.059 V $pH^{-1}$.

The dissimilar proton activity dependence on supporting electrolyte concentration for the acidic, buffered, and alkaline electrolytes studied can be understood through differential interaction between dissolved protic ($H_3O^+$, $OH^-$) and aprotic ($Na^+$, $ClO_4^-$) ions. Changes in water activity alone, which span only a factor of two between 1 m and 17m,[57,59] are insufficient to account for observed changes in $E_{RHE}$ (**Equation 1**). The large positive shift in $E_{RHE}$ of the $HClO_4$ electrolytes evinces a differential increase in the activity of $H_3O^+$ relative to water as $NaClO_4$ concentration increases. This increase in activity can be rationalized in terms of an increasing competition between $H_3O^+$ and $Na^+$ for solvent molecules, resulting in the destabilization of $H_3O^+$ relative to water. On the other hand, competition for solvent molecules is less perturbative in alkaline media as $OH^-$ is more weakly solvated than $H_3O^+$, a general property of anions,[47,48,56,60] resulting in the minimal observed change in $E_{RHE}$. Likewise, in acetate buffered solution, the solution pH is set by the activities of AcOH and $AcO^-$ which, as a neutral and anionic species are also weakly solvated compared to $H_3O^+$, resulting in a similar conservation of $E_{RHE}$ across the studied ionic strength range.

## Effect of ionic-strength on I-PCET thermodynamics at GC-COOH

With an understanding of the bulk activities of proton donors and acceptors in hand, we employed GC-COOH electrodes to study the effects of electrolyte concentration on the thermodynamics of elementary interfacial electrochemical reactions. GC-COOH electrodes were prepared by heating glassy carbon plates in an ethanolic solution of 3,4-diaminobenzoic acid (**Figure 3a**). Upon application of a negative potential GC-COOH carboxylate active sites bind protons, enforcing electron redistribution within the electrode, constituting an interfacial proton-coupled electron transfer reaction. As these sites are well defined and consistent, the surface-proton bonds formed are uniform and have a defined bond strength. **Figure 3b** depicts the I-PCET reaction at GC-COOH's carboxylate site for an unspecified proton

donor. The overall reaction at GC-COOH when the bulk proton activity is set by the $H_3O^+$/ $H_2O$ couple is:

$$GC\text{-}COO^- + H_3O^+ + e^- \rightleftharpoons e^-/GC\text{-}COO\text{-}H + H_2O \qquad \textbf{Reaction 3}$$

When set by the $AcOH/AcO^-$ couple, it is:

$$GC\text{-}COO^- + AcOH + e^- \rightleftharpoons e^-/GC\text{-}COO\text{-}H + AcO^- \qquad \textbf{Reaction 4}$$

And when set by the $H_2O/OH^-$ couple, it is:

$$GC\text{-}COO^- + H_2O + e^- \rightleftharpoons e^-/GC\text{-}COO\text{-}H + OH^- \qquad \textbf{Reaction 5}$$

where $GC\text{-}COO^-$ represents the deprotonated carboxylic acid site with an accompanying hole and $e^-/GC\text{-}COO\text{-}H$ represents the protonated site with an accompanying electron in the electrodes band states. Comparing **Reaction 3** through **Reaction 5** to **Reaction 1** and **Reaction 2** highlights that proton binding at GC-COOH and the HER/HOR are both I-PCET reactions with identical proton/electron stoichiometry and terminal proton donor/acceptors dependencies. As detailed previously,[38–40] the molecularly defined structure and position within the EDL of GC-COOH active sites make these electrodes particularly well suited to investigating on-electrode ion-transfer reactions.

The equilibrium thermodynamics of I-PCET at GC-COOH were quantified at each solution condition using slow scan-rate cyclic voltammetry. **Figure 3c** shows a cyclic voltammogram (CV) of GC-COOH in an electrolyte containing 1 m $NaClO_4$ plus 0.1 M NaOH, with a pH of 12.6, as measured by both a pH probe and $E_{RHE}$. Starting from 0 V vs SHE the GC-COOH active sites are entirely deprotonated. Upon application of a reducing potential, the electrochemical proton affinity of the surface sites increases, causing the carboxylic acid to bind a proton at −0.45 V vs SHE.[38,40] To maintain the electrostatic potential of the electrode, as the proton crosses the EDL to bind to the surface a compensatory electron must flow from the external circuit to maintain the potential of the electrode. This electron flow is evidenced in the CV by the reductive wave at this potential. Polarizing to more negative potentials causes the two slightly Brønsted basic pyrazine nitrogen atoms to each bind a proton as well. The peaks near −0.65 V corresponding to the pyrazine I-PCET are twice as large as the carboxylate peak, given the two-to-one ratio of pyrazine nitrogen atom to carboxylic acid sites. Sweeping from negative to positive potentials raises the sites' effective p$K_a$ values, first deprotonating the pyrazines at −0.65 V and the carboxylic acid moiety at −0.45 V. The mean of the peak cathodic and anodic peak potentials corresponding to the I-PCET at the surface carboxylate was taken as the reaction's equilibrium potential.

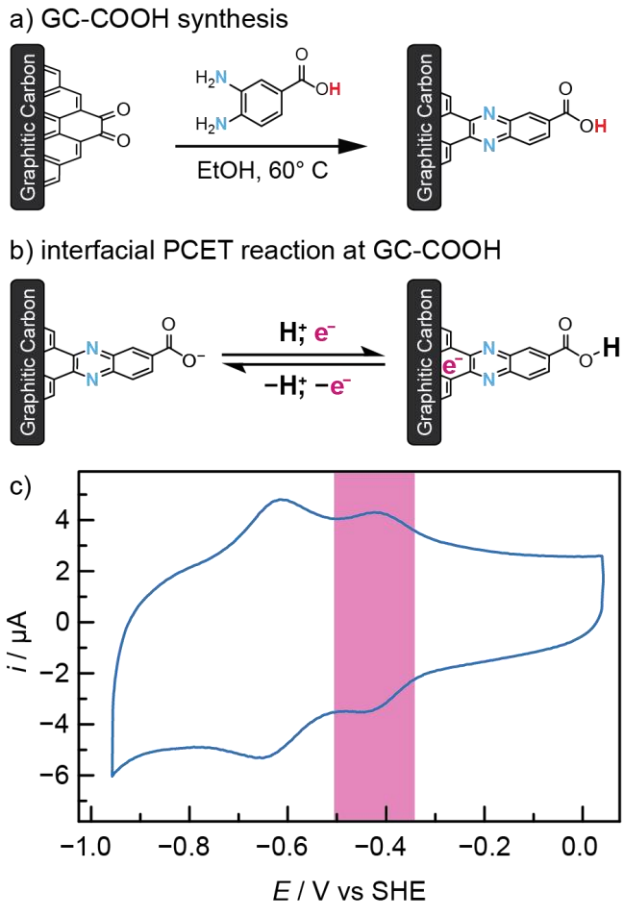


**Figure 3 | GC-COOH preparation, I-PCET reactivity, and a cyclic voltammogram (CV). a) Illustration of the condensation of 3,4-diaminobanzoic acid to an *ortho*-quinone moiety of glassy carbon to produce a GC-COOH site. b) I-PCET at a GC-COOH site showing, upon application of a reducing potential, formation of a chemical bond of a proton from solution to the GC-COOH site coupled to delocalized compensatory charge flow into the electrode, represented by "e⁻". c) CV of the reaction in 1 m $NaClO_4$ plus 0.1 M NaOH electrolyte showing pyrazine I-PCET peaks at −0.65 V vs SHE and carboxylate I-PCET at −0.4 V vs SHE shaded pink.**

The supporting-electrolyte-concentration dependence of I-PCET thermochemistry was assessed by measuring equilibrium potentials ($E^{eq}$) of I-PCET at GC-COOH at the same proton donor and electrolyte conditions of the above $E_{RHE}$ measurements. **Figure 4** displays carboxylate I-PCET $E^{eq}$ values as a function of $NaClO_4$ concentration for the same acidic, buffered, and basic proton donor conditions as in the above $E_{RHE}$ studies (See **Supplementary Data 1** for representative cyclic voltammograms from each condition.) **Figure 4a** shows $E^{eq}$ for I-PCET referenced to the pH independent SHE scale. In the presence of 1 m $NaClO_4$, $E^{eq}$ occurred at 0.34 V vs SHE for the acidic electrolyte, 0.12 V vs SHE for the buffered electrolyte, and −0.42 V vs SHE for the alkaline electrolyte. These $E^{eq}$ values at ~1.1 M total ionic strength are within a few millivolts of the expected $E^{eq}$ vs $E_{RHE}$ measured previously for a 1 M solution.[38] As ionic strength increased from 1 m to 17 m $NaClO_4$, $E^{eq}$ for the acidic electrolytes increased significantly to 0.49 V vs SHE, whereas $E^{eq}$ for the buffered and alkaline electrolytes decreased only slightly to −0.09 V vs SHE and −0.46 V vs SHE, respectively. These changes are similar to the $E_{RHE}$ shifts observed in **Figure 2**. The commensurate slopes of the $E^{eq}$ vs molality and $E_{RHE}$ vs molality trends are unsurprising as both I-PCET reactions have the same electron/proton stoichiometry.

To account for the expected proton activity dependence of GC-COOH I-PCET and reveal possible deviations in the two reactions' concentration dependences, it is helpful to reference $E^{eq}$ to the proton-activity-dependent $E_{RHE}$ measurements in **Figure 2** for each condition, as shown in **Figure 4b**. Starting from the 1 m $NaClO_4$ condition, $E^{eq}$ equals 0.40 V vs RHE for the acidic electrolyte, 0.38 V vs RHE for the buffered electrolyte, and 0.32 V vs RHE for the alkaline electrolyte. Transiting from 1 m to 17 m**Figure 4** shows only slightly divergent behavior. For the acidic electrolyte ($E^{eq} - E_{RHE}$) increased by 29 mV, whereas for the buffered and alkaline electrolytes ($E^{eq} - E_{RHE}$) decreasesd by 10 mV and 21 mV, respectively. Such small discrepancies in $E^{eq}$ over an enormous range of electrolyte concentrations indicate that the equilibria of I-PCET and relative surface site activities of GC-COOH track with proton activity largely as expected from the reactions' proton donor/acceptor stoichiometry.

The remaining small changes in ($E^{eq} - E_{RHE}$) could potentially result from minor variation in surface-hydrogen bond dissociation free energy (H-BDFE). Notably, a slight deviation from strictly Nernstian scaling between $E^{eq}$ and pH (−64 mV $pH^{-1}$ vs −59 mV $pH^{-1}$), as previously reported,[38] gives rise to the difference in ($E^{eq} - E_{RHE}$) at 1 m supporting electrolyte. Thus, the accentuation of this difference at higher electrolyte strength can be seen as largely arising from this super-Nernstian scaling acting upon the spread in pH. Additionally, some of the shift in ($E^{eq} - E_{RHE}$) might arise from potential-dependent changes in the populations of ions at the interfaces. GC-COOH electrodes have been shown to be equipotential with aqueous media near 0.1 V vs SHE (at the potential of zero free charge or $E_{PZFC}$).[40] In the acidic media studied, positive of $E_{PZFC,}$ the electrostatic potential drop is expected to draw a negative charge from the electrolyte toward the electrode surface. The increasing enrichment in interfacial $ClO_4^-$ could serve to donate increasing charge into the carboxylic acid moieties with increasing ionic strength, making the sites slightly more basic, slightly strengthening their H-BDFE and increasing ($E^{eq} - E_{RHE}$). Conversely, for the basic electrolytes, negative of $E_{PZFC}$, a deepening electrostatic potential drop will enrich the interface with $Na^+$ ions, withdrawing charge from the carboxylate moieties, slightly acidifying them, marginally lowering their H-BDFE, and decreasing ($E^{eq} - E_{RHE}$). Lastly, for the acetate buffered electrolytes, near $E_{PZFC}$, the constancy of interfacial electrostatic potential across the interface means inductive effects into the electrode is unaffected by ionic strength and H-HDFE is unperturbed. In any case, a 30 mV shift amounts to at most a 0.7 kcal $mol^{-1}$ change in H-BDFE, a rather modest deviation for such significant change in electrolyte properties and water structure. The tracking of $E^{eq}$ with $E_{RHE}$ suggests changes in overall ionic strength result in relatively minor differences in I-PCET thermodynamics and surface site speciation from the dilute to saturated regimes when corrected for the change in proton activity.

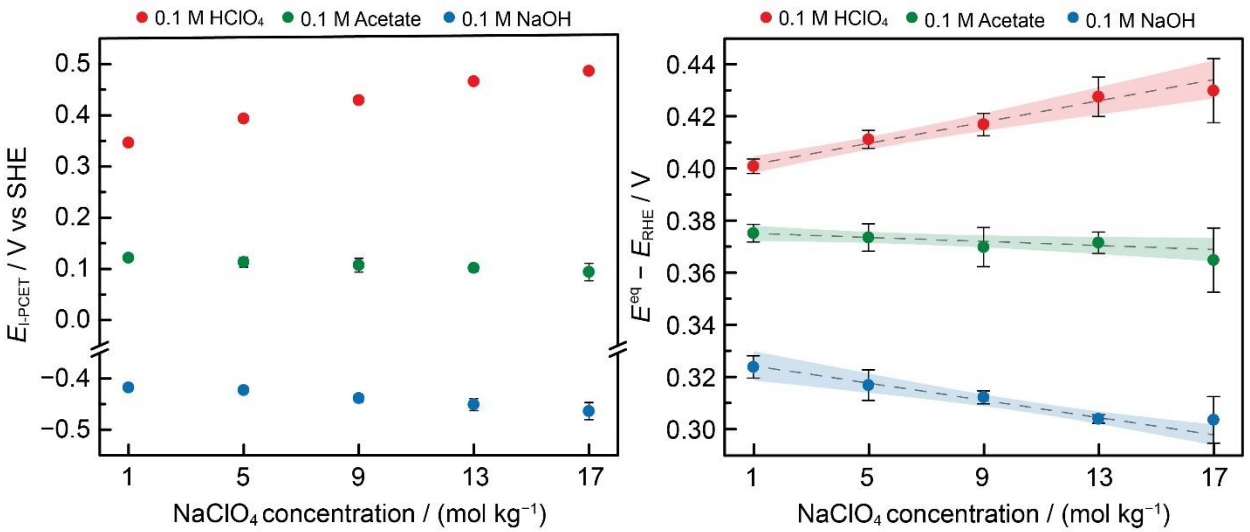


**Figure 4 | Potential of I-PCET at GC-COOH as a function of $NaClO_4$ concentration referenced to SHE (left) and RHE (right).** $E^{eq}$ in solutions from 1 m to 17 m $NaClO_4$ with solution proton activity set by 0.1 M $HClO_4$ (red), acetate buffer (green), and NaOH (blue). Left: $E^{eq}$ referenced versus the pH independent SHE scale. Right: $E^{eq}$ referenced to the proton-activity-dependent RHE scale by subtracting the $E_{RHE}$ potentials defined in **Figure 2** from $E^{eq}$ in the left panel to account for concentration-dependent proton activity. Points are means of three measurements, error bars represent 2σ, dotted gray lines represent linear regressions, and shaded regions represent 95% confidence band of each data set.

## Effect of ionic strength on I-PCET kinetics

With an understanding of I-PCET thermodynamics at GC-COOH electrodes, we sought to investigate the mechanism of I-PCET. This was achieved by measuring I-PCET kinetics as a function of ionic strength and ionic-strength-dependent proton activity using the method of Laviron, also known as trumpet plot analysis.[30,38,61] In the method of Laviron, for a surface confined electron transfer reaction CVs such as in **Figure 3** are collected across several orders of magnitude in scan rate. As scan rate increases to a point where the surface reaction is out of equilibrium, the CV's anodic and cathodic peak potentials ($E_{peak}$) begin to separate.[29] Plotting the equilibrium-potential-normalized peak potentials ($E_{peak} - E^{eq}$) as a function of scan rate results in a characteristic trumpet shape (**Figure 5**, top)**.** The experimental $E_{peak} - E^{eq}$ data in the trumpet plots can then be fit to the $E_{peak} - E^{eq}$ points of simulated CVs (**Figure 5** top, purple arc) to extract site normalized apparent rate constants ($k_{app}$ in $s^{-1}$) describing the equilibrium (zero overpotential) exchange rate of I-PCET. Our previous report presents a detailed explanation of this method and its application to I-PCET at GC-COOH.**[38]**

Across solutions of constant ionic strength, we previously showed that the kinetics of I-PCET at GC-COOH are highly dependent on solution pH, with I-PCET being fastest at pH extremes and slowest at intermediate pH. Derived from simple linear-free-energy rate-potential dependencies, our mechanistic approach faithfully captures the observed dependence over three orders of magnitude in apparent rate constant and fourteen orders of magnitude in proton activity. In our model, dubbed the caldera model given the rate dependency's inverted-volcano shape, the overall apparent rate constant, $k_{app}$, is simply the sum of the individual pH-dependent apparent rate constants for I-PCET with two separate proton donor/acceptor couples (**Figure 5** bottom, green). One couple consists of $H_3O^+$ as the proton donor for I-PCET and water as the conjugate acceptor (the "acid" reaction, equivalent to **Reaction 3**), while the other consists of water as the proton donor and $OH^-$ as the conjugate acceptor (the "base" reaction,

equivalent to **Reaction 5**). In acidic conditions where the activity of $H_3O^+$ far outweighs $OH^-$, the acid reaction prevails and its component pH-dependent apparent rate constant, $k_{app,acid}$(pH) (**Figure 5** bottom, red) far exceeds that of the $H_2O/OH^-$ couple, $k_{app,base}$(pH) (**Figure 5** bottom, blue). Alternatively, in alkaline conditions, $OH^-$ activity far exceeds $H_3O^+$ activity and $k_{app,base}$ is larger. While other buffering species may be present in solution, we showed that at GC-COOH acetic acid and acetate serve only to set solution pH and are not competent proton donors or acceptors. Therefore **Reaction 4** governs the overall thermochemistry but does not control the rate of I-PCET. As derived in our previous study, the two pH-dependent component apparent rate constants are each a function of only two parameters, the rate constant at standard state ($k^0_{acid}$ at pH 0 for acid, and $k^0_{base}$ at pH 14 for base) and a linear-free-energy scaling constant for each reaction ($\alpha_{acid}$ for the acid reaction and $\alpha_{base}$ for the base reaction). The overall caldera-shaped pH dependence can be written as:

$$k_{app}(\mathrm{pH}) = k_{app,acid}(\mathrm{pH}) + k_{app,base}(\mathrm{pH}) \qquad \textbf{Equation 5}$$

$$k_{app,acid}(\mathrm{pH}) = k^0_{acid}10^{-(1-\alpha_{acid})\mathrm{pH}} \qquad \textbf{Equation 6}$$

$$k_{app,base}(\mathrm{pH}) = k^0_{base}10^{\alpha_{base}(\mathrm{pH}-\mathrm{p}K_w)} \qquad \textbf{Equation 7}$$

$$k_{app}(\mathrm{pH}) = k^0_{acid}10^{-(1-\alpha_{acid})\mathrm{pH}} + k^0_{base}10^{\alpha_{base}(\mathrm{pH}-\mathrm{p}K_w)} \qquad \textbf{Equation 8}$$

In our previous study, the four governing parameters were determined to be $k^0_a$ = 21,000 $s^{-1}$, $k^0_b$ = 5,000 $s^{-1}$, $\alpha_a$ = 0.66, and $\alpha_b$ = 0.70 for I-PCET at GC-COOH. While the caldera model successfully captures the kinetic pH dependence of moderately dilute solutions, it was not developed to predict how electrolyte concentration controls I-PCET rates.

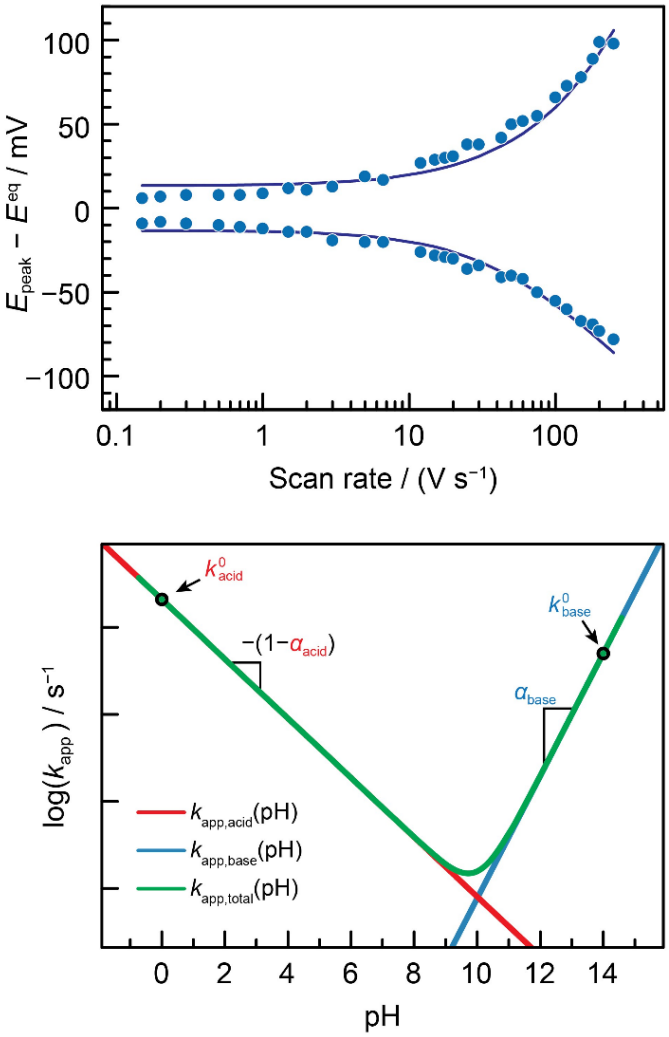


**Figure 5 | Representative trumpet plot (top) and idealized $k_{app}$ vs pH dependence expected from the caldera model at constant ionic strength (bottom). top)** A trumpet plot depicting the separation of peak potentials from the equilibrium potential ($E_{peak} - E^{eq}$) as a function of scan rate for I-PCET at GC-COOH in 1 m $NaClO_4$ + 0.1 NaOH. (pH 12.6) Blue dots represent measured potentials and purple arcs represent simulated best fit peak positions for CVs with $k_{app}$ = 770 $s^{-1}$ for this particular data set. **right**) Representation of caldera model for I-PCET at GC-COOH across pH values at 1 molar total ionic strength.[22] The "V" shape of the total observed rate constant $k_{app,total}$(pH) is the sum of those for the acid and base reactions. The acid component $k_{app,acid}$(pH) is shown in red, anchored at pH 0 by $k^0_{acid}$ with a pH dependence log-linear with –(1–$\alpha_{acid}$) and the base component $k_{app,acid}$(pH) is shown in blue, anchored at pH 14 by $k^0_{base}$ with a pH dependence log-linear with $\alpha_{base}$.

**Figure 6a** shows $k_{app}$ values extracted from trumpet plots for the three proton donor/acceptor conditions from 1 m to 17 m $NaClO_4$. (See **Supplementary Data 2** for representative trumpet plot from each condition.) Starting from the 1 m $NaClO_4$ condition, $k_{app}$ values extracted based on linear regression equal 9200 ± 1700 $s^{-1}$ for the acidic condition, 1300 ± 460 $s^{-1}$ for the buffered condition, and 920 ± 240 $s^{-1}$ for the basic condition. These values are very close to those expected from the caldera model for a ~1 m solution. Traversing the range in electrolyte concentrations, the values of $k_{app}$ as a function of concentration are best understood on a logarithmic scale. For acidic conditions, $k_{app}$ is essentially unchanged at $10^{3.97}$ $s^{-1}$

for all ionic strengths studied. This differs from the observation for acetate buffered electrolytes where $k_{app}$ decreases from $10^{3.11}$ $s^{-1}$ at 1 m to $10^{2.36}$ $s^{-1}$ at 17 m, a factor of ~5.5. Lastly, $k_{app}$ values obtained for alkaline media increases only slightly from $10^{2.96}$ at 1 m to $10^{3.09}$ at 17 m, all within experimental error of each other and of the value measured at pH 13 in the caldera study.[38] Upon cursory examination, the kinetics of I-PCET seem to be independent of ionic strength in unbuffered acidic and alkaline media whereas in buffered media I-PCET slows with increasing ionic strength. However, when these *insignificant changes in* $k_{app}$ based on ionic strength for acidic electrolytes are viewed in context of the associated *significant changes in* $pH_{eff}$ (**Figure 2**, red) and, similarly, the *significant changes in* $k_{app}$ for the acetate buffered electrolytes are viewed in the context of *insignificant changes in* $pH_{eff}$, (**Figure 2**, green) it is apparent that an ionic-strength-dependent factor beyond proton activity must control I-PCET rates in concentrated media.

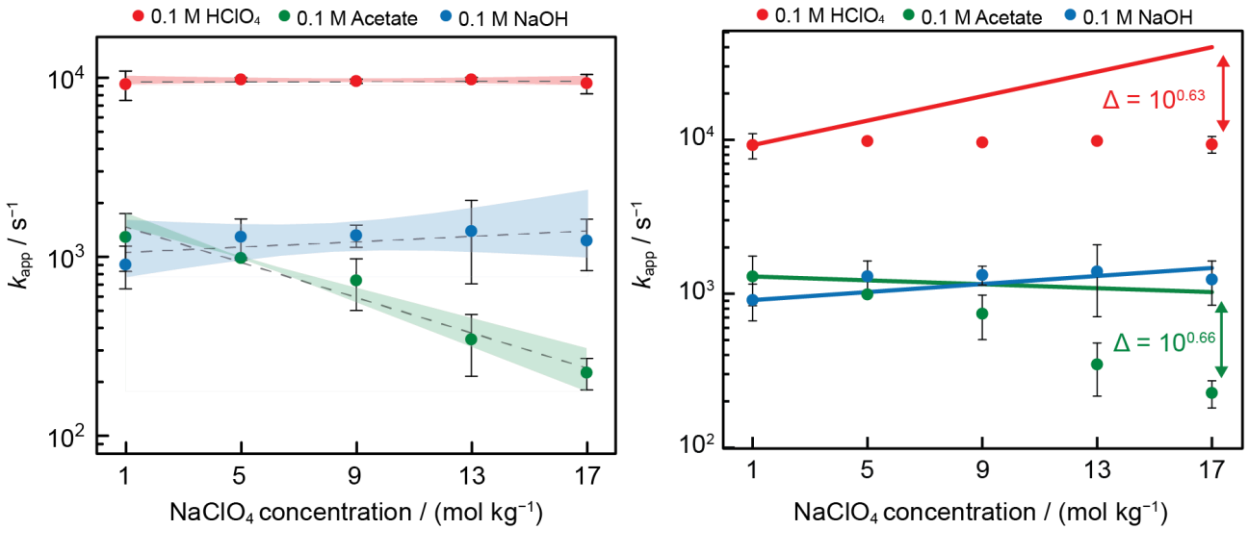


**Figure 6 | Apparent rate constant** ***($k_{app}$)*** **for I-PCET at GC-COOH as a function of electrolyte concentration. a)** Values of $k_{app}$ extracted from trumpet plots for each of three proton donor/acceptor conditions are plotted as a function of molality. Values for 0.1 M $HClO_4$ (red) and 0.1 M NaOH (blue) are largely independent of ionic strength, while for 0.1 M acetate buffer (green) there is a marked decrease in rate at higher $NaClO_4$ concentrations. Points are means of three measurements; error bars represent 2σ, dotted gray lines represent linear regressions, and shaded regions represent 95% confidence band of each data set. **b)** Values of $k_{app}$ from panel a (circles) and predicted ionic strength dependence of $k_{app}$ based on changes in $pH_{eff}$ (lines) calculated by adjusting the measured 1 m value using the estimated change in $pH_{eff}$ from **Figure 2** regressions and appropriate scaling coefficient α from **Figure 5**.

Careful examination of the trends in $E_{RHE}$ trends shown in **Figure 2** and I-PCET rate constants shown in **Figure 6a** reveals an unexpected symmetry between the increase of $E_{RHE}$ for acidic solutions and the decrease in $k_{app}$ for buffered solutions. For acidic electrolytes, a linear regression of $E_{RHE}$ against concentration predicts an increase in $E_{RHE}$ equivalent to a 1.9 unit decrease in $pH_{eff}$ as the concentration is increased from 1 m $NaClO_4$ to 17 m $NaClO_4$. According to **Equation 6** and assuming $\alpha_a = 0.66$, this pH decrease corresponds to an increase $k_{app}$ of 0.64 log units, in sharp contrast to the measured increase of 0.01 log units (**Figure 6b**, red). On the other hand, an analogous linear regression for the buffered system of $E_{RHE}$ against concentration predicts a smaller decrease in $E_{RHE}$ equivalent to a 0.3 unit increase in $pH_{eff}$ as the concentration is increased from 1 m $NaClO_4$ to 17 m $NaClO_4$. In contrast to the relatively small $k_{app}$

decrease of 0.10 log units predicted by **Equation 6** ($\alpha_a = 0.66$) for such a pH change, the observed change in $k_{app}$ is a decrease of 0.76 log units, resulting in a very similar *relative* $k_{app}$ decrease of 0.66 log units (**Figure 6b**, green). Thus, it can be observed that in both cases the observed rate is lower than would be predicted based on $pH_{eff}$ alone, whether this manifests as a decrease in the observed $k_{app}$ (as in buffered solution) or as the failure to observe an expected increase in $k_{app}$ (as in acidic solution). Moreover, the relative rate decrease is similar in both cases, corresponding to an effective pH increase of ~2 units. These observations demonstrate that the observed kinetic changes cannot be rationalized exclusively by applying our pre-existing kinetic model to measured changes in $E_{RHE}$ to capture changes in effective pH, and the striking similarity between the relative rate decreases as a function of ionic strength in acidic and buffered media suggests a common effect might govern the deviations from expected behavior in both systems.

# Model

To explain the decrease in I-PCET rate constants relative to that expected based on the caldera model, we introduce a complementary mechanistic model for I-PCET that explicitly accounts for the need to form a pre-association complex prior to CPET. This model must account for the three different conditions studied and capture the key observations of an absolute rate decrease in the acetate-buffered electrolyte and a relative rate decrease (upon accounting for the $pH_{eff}$-predicted rate) in acidic electrolyte.

The decrease in I-PCET rates relative to molality-dependent proton activity, $pH_{eff}$, in acidic and buffered concentrated $NaClO_4$ electrolytes must stem from a negative order in the concentration of the supporting electrolyte ions. Activity changes associated with the terminal reactive species in **Reaction 3** through **Reaction 5** cannot account for the observed trend. The effect of the proton donor/acceptor activity changes have already been accounted for in adjusting for $pH_{eff}$. The surface activities of protonated (GC-COOH) and deprotonated ($GC\text{-}COO^-$) sites are equal to each other by virtue of sampling the rate at the equilibrium potential, which itself changes minimally across the $NaClO_4$ concentration range relative to $E_{RHE}$ (**Figure 4**). Consequently, we invoked that the increase in the $Na^+$ and $ClO_4^-$ ion activities themselves are the principal origin of the observed attenuation in I-PCET kinetics.

To account for the kinetic dependence on $NaClO_4$ concentration, we propose an I-PCET reaction mechanism in which the rate-limiting elementary CPET occurs from a hydrogen-bonded pre-association complex (**Figure 7**). In acid (**Reaction 3**), the putative pre-association complex for the forward reaction consists of a hydronium ion hydrogen bonded to $GC\text{-}COO^-$ and the corresponding pre-association complex for the reverse reaction consists of a water molecule hydrogen bonded to GC-COOH. Importantly, this model invokes that the formation of both these pre-association complexes (in both directions) require the displacement of $Na^+$ from the interface to the bulk medium. Thus, the equilibrium constant for forming these pre-association complexes is expected to depend on the relative changes in interfacial vs bulk $Na^+$ activity as a function of $NaClO_4$ concentration. Notably, even for relatively dilute bulk solution concentrations, the thin layer of solution where a solid electrode and liquid electrolyte meet reaches solute concentrations far exceeding the same ions' saturation concentration in the associated bulk solution by up to eighty-fold.[62,63] Electrochemical impedance measurements of copper electrodes further indicate that at constant potential, the interfacial capacitance of $NaClO_4$ electrolytes are nearly constant from 0.5 m to 17 m.[57] While the EDL structure for our graphitic electrodes likely differ from that of copper electrodes and the inference of thermodynamic properties from capacitance is complex, the above findings, taken together, suggest that the charge density and structure of the EDL remains largely unchanged across the large electrolyte concentration range probed in this study. This putative uniformity in interfacial $NaClO_4$ activity stands in stark contrast to the enormous change in solution activity from 1 m to 17 m $NaClO_4$, equal to a change in electrolyte mole fraction from 1.8% to 23% alongside a 50% increase in activity coefficient.[64] Consequently, we invoke that increased $NaClO_4$ concentration serves

increase $Na^+$ activity in the bulk relative to the interface, thereby inhibiting the $Na^+$ displacement required for formation of the pre-association complexes. For a more detailed discussion concerning the presence of charge-matched co-ions at the interface, see **Supplementary Note 4.**

To include pre-rate limiting interfacial co-ion rearrangement in the hydronium-donor I-PCET, as occurs in both in the $HClO_4$ and acetate buffered electrolytes, **Reaction 3** can be expanded to three steps:

$$\begin{aligned} GC\text{-}COO^- + Na^+_{int} + H_3O^+_{bulk} &\rightleftharpoons \\ GC\text{-}COO^- + H_3O^+_{int} + Na^+_{bulk} &\overset{e^-}{\rightleftharpoons} e^-/GC\text{-}COOH + H_2O_{int} + Na^+_{bulk} \\ &\rightleftharpoons e^-/GC\text{-}COOH + Na^+_{int} + H_2O_{bulk} \end{aligned} \qquad \textbf{Reaction 6}$$

Where the subscript "int" indicates an interfacial species. **Reaction 6**, shown pictorially in **Figure 7**, includes (1) a $Na^+$ ion leaving the interface before PCET to accommodate a $H_3O^+$donor, (2) the I-PCET reaction step, as well as (3) an $Na^+$ ion returning to the interface following the PCET step. As discussed previously,[38] the I-PCET step itself contains three elementary steps, (2a) the formation of a hydrogen-bonded pre-association complex containing the proton donor and deprotonated active site, (2b) the CPET step within the pre-association complex, and (2c) scission of the successor complex to the protonated active site and conjugate proton acceptor. **Reaction 6** requires $Na^+$ to return to the EDL following I-PCET because the neutralization of the cationic $H_3O^+$ during I-PCET creates a charge imbalance near the interface. As $Na^+_{int} \rightleftharpoons Na^+_{bulk}$ precedes the rate limiting step, the overall reaction slows as the activity of $Na^+_{bulk}$ increases relative to $Na^+_{int}$. Conversely, the concluding step $Na^+_{bulk} \rightleftharpoons Na^+_{int}$ should become more favorable with increased $Na^+_{bulk}$, but this equilibrium follows the rate limiting step and therefore does not affect the overall rate of **Reaction 6**. Likewise, in the reverse direction, the microscopic reverse of step (3) ($Na^+_{int} + H_2O_{bulk} \rightleftharpoons H_2O_{int} + Na^+_{bulk}$) precedes the rate-limiting I-PCET step, imposing the same pre-rate limiting dependence on interfacial ion transfer in the reverse I-PCET pathway. As I-PCET rates are measured near equilibrium, the reverse I-PCET, deprotonation by water, must also account for $Na^+$ ion movement out of the interface preceding the rate-limiting I-PCET.

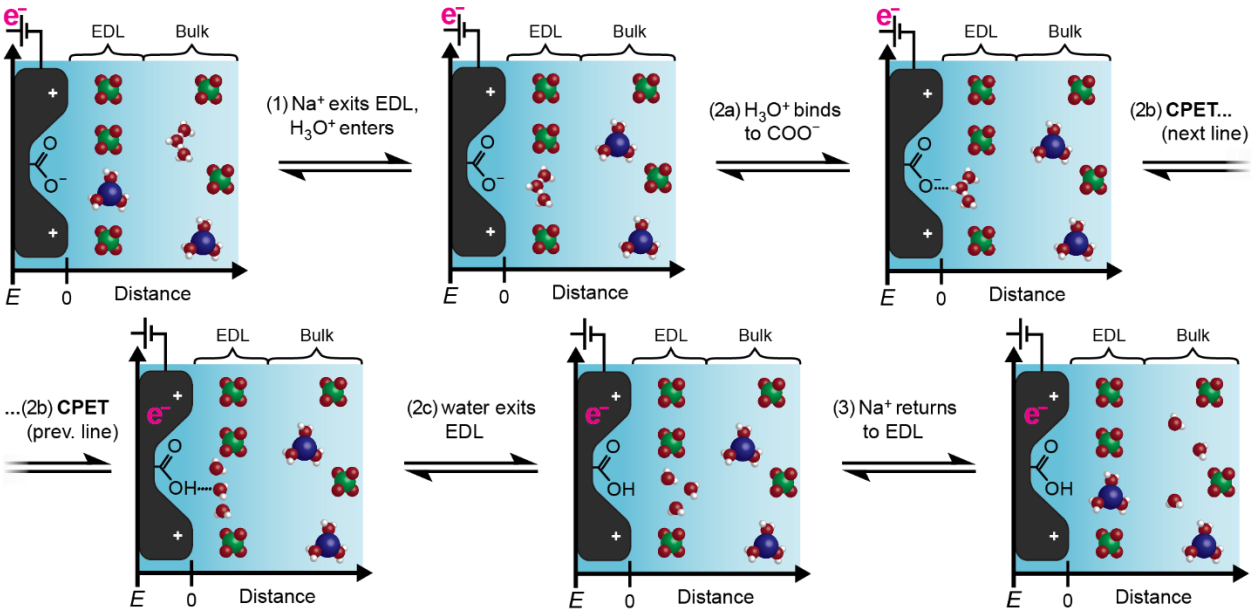


**Figure 7 | Five elementary sub-steps of I-PCET when $H_3O^+$ acts as the proton donor to the surface carboxylic acid site.** (1) A $Na^+$ near the interface leaves the EDL, permitting a $H_3O^+$ to enter the EDL. (2a) $H_3O^+$ from the EDL specifically adsorbs to the carboxylate surface site in a hydrogen bonded I-PCET pre-association complex. (2b) Concerted proton electron transfer within the pre-association complex: a proton transfers from the $H_3O^+$ donor to the surface carboxylate, leaving behind a hydrogen bonded water molecule, the conjugate proton acceptor. Meanwhile, an electron flows from the external circuit to counteract the proton's charge. Since electron motion within the conductive circuit is effectively barrierless, these two charge transfers occur in a single step. (2c) The successor complex cleaves, as water transits back to the EDL. (3) A $Na^+$ ion returns to the EDL to reestablish the charge state present before I-PCET.

In alkaline media where $OH^-$ acts as a proton acceptor, **Reaction 5** can be expanded to include anion movement just as **Reaction 3** is expanded to include cation movement in **Reaction 6**. In this case it is helpful to write out the I-PCET in the reverse direction with $OH^-$ accepting a proton from the surface.

$$e^-/\text{GC-COOH} + ClO^-_{4,int} + OH^-_{bulk} \rightleftharpoons$$

$$e^-/\text{GC-COOH} + OH^-_{int} + ClO^-_{4,bulk} \overset{-e^-}{\rightleftharpoons} \text{GC-COO}^- + H_2O_{int} + ClO^-_{4,bulk}$$

$$\rightleftharpoons \text{GC-COO}^- + ClO^-_{4,int} + H_2O_{bulk} \qquad \textbf{Reaction 7}$$

**Reaction 7** involves the displacement of interfacial $ClO_4^-$ by $OH^-$ from the bulk preceding the rate limiting I-PCET step as well as a subsequent return of anionic $ClO_4^-$ to the EDL. Just as in **Reaction 6**, the post-rate-limiting return of $ClO_4^-$ to the EDL is needed to reestablish interfacial charge neutrality and ensure that the microscopic reverse of **Reaction 7** also involves pre-rate-limiting interfacial ion displacement.

To account for pre-rate-limiting interfacial-co-ion transfer on I-PCET rates, we introduce complementary ionic-strength-dependent rate equations to those of **Equation 6** and **Equation 7** that

define the constant ionic-strength caldera model. Incorporating an inverse dependence of I-PCET's apparent rate constant on the ratio of bulk to interfacial $NaClO_4$ activity results in the following equations:

$$k_{\mathrm{app,acid}}(\mathrm{pH_{eff}}, m) = k^0_{\mathrm{acid}} \times \frac{a^{\mathrm{int}}_{\mathrm{Na^+}}(m)}{a^{\mathrm{bulk}}_{\mathrm{Na^+}}(m)} a^{\mathrm{bulk}}_{\mathrm{H_2O}}(m) \times 10^{-(1-\alpha_{\mathrm{acid}})\mathrm{pH_{eff}}} \quad \textbf{Equation 9}$$

$$k_{\mathrm{app,base}}(\mathrm{pH_{eff}}, m) = k^0_{\mathrm{base}} \times \frac{a^{\mathrm{int}}_{\mathrm{ClO_4^-}}(m)}{a^{\mathrm{bulk}}_{\mathrm{ClO_4^-}}(m)} a^{\mathrm{bulk}}_{\mathrm{H_2O}}(m) \times 10^{\alpha_{\mathrm{base}}(\mathrm{pH_{eff}}-\mathrm{p}K_{\mathrm{w}})} \quad \textbf{Equation 10}$$

The "*a*" terms refer to the activity of the subscripted species in either the superscripted bulk or interfacial phase. Each *activity* term and apparent rate constant, $k_{app}$, term is noted as a function of the bulk supporting electrolyte molality "*m*," with each term separately dependent on the bulk ion *concentration*. A full derivation of **Equation 9** and **Equation 10**, including the explicit dependence on water activity appear in the **Supplementary Note 2** and **Supplementary Note 3.** Defining the bulk ion activities and the bulk activity of water to be unity at 1 mol $kg^{-1}$ ionic strength and referencing the unknown interfacial ion activities as unity as well, **Equation 9** and **Equation 10** collapse into **Equation 6** and **Equation 7** that define apparent rate constant at 1 molal ionic strength. The proposed interfacial ion transfer reactions, though operative at these lower concentrations, only exert apparent rate control when I-PCET rates are measured over a large range of ion strength conditions. As written, it is clear that an increase in bulk ion activity relative to the interfacial ion and bulk water activities leads to an overall rate decrease as ionic strength increases at a fixed pH.

Differing dependencies between bulk vs. interfacial activities for $ClO_4^-$ ions and bulk vs. interfacial activity for $Na^+$ ions on bulk sodium perchlorate concentration give rise to the more muted scaling of observed I-PCET rates versus $pH_{eff}$ in the basic electrolytes. As mentioned above, at 17 m in both electrolytes where $H_3O^+$ acts as the proton donor the apparent rate constant for I-PCET is about 4.5-times less than would be expected from **Equation 6** for the measured proton activity (Error! Reference source not found., red & green). The complementary factors included in **Equation 9**, but not **Equation 6**, that is $\frac{a^{\mathrm{int}}_{\mathrm{Na^+}}(m)}{a^{\mathrm{bulk}}_{\mathrm{Na^+}}(m)} \times a^{\mathrm{bulk}}_{\mathrm{H_2O}}(m)$, must account for this change. According to this model, in light of the 2-fold decrease in $a^{\mathrm{bulk}}_{\mathrm{H_2O}}(m)$ from 1 m to 17 m $NaClO_4$,[59] a ~2.25-fold increase of $a^{\mathrm{bulk}}_{\mathrm{Na^+}}(m)$ compared to $a^{\mathrm{int}}_{\mathrm{Na^+}}(m)$ over the same range must be hindering rate-limiting ion transfer and slowing I-PCET at high ionic strength. Notably, this scaling in bulk and interfacial $Na^+$ activity differs only minutely between the acetate buffered electrolytes at 0 V vs $E_{PZFC}$ and $HClO_4$ electrolytes at least 0.25 V positive of $E_{PZFC}$, two cases where the EDL structure could differ significantly. In basic media, the change in $k_{app}$ tracks more closely to the 2-fold increase predicted by **Equation 7**, suggesting that changes in $\frac{a^{\mathrm{int}}_{\mathrm{ClO_4^-}}(m)}{a^{\mathrm{bulk}}_{\mathrm{ClO_4^-}}(m)} \times a^{\mathrm{bulk}}_{\mathrm{H_2O}}(m)$ are comparatively minor (**Figure 6b**, blue).

The stark difference in interfacial versus bulk activity scaling for the $Na^+$ and $ClO_4^-$ ions likely stems from different solvation thermodynamics between the more charge-dense cation and diffusely charged anion.[47,56] Competition for solvation increases the chemical activity of bulk $Na^+$ ions, impeding the transit of $Na^+$ ions away from the interface and inhibiting the approach of $H_3O^+$ to the GC-COOH active site (Error! Reference source not found., left). Conversely, the more diffusely charged $ClO_4^-$ is less destabilized by the paucity of solvent, resulting in a minimal change in $ClO_4^-$ activity in the bulk from 1 m to 17 m $NaClO_4$ and thus limited sluggishness arising from pre-rate-limiting ion transfer when $OH^-$ acts a proton

acceptor. The minimal changes in pre-rate-limiting interfacial ion transfer and rate-limiting I-PCET equilibria lead to no net change in apparent I-PCET rates **(Figure 8**, right). Indeed, though impossible to verify experimentally,[58] computational models suggest $Na^+$ and $ClO_4^-$ could have asymmetric individual ion activity coefficients in the bulk.[65–67] Though the magnitudes of the effective rate increase due to donor/acceptor activity and the effective rate decrease due to the product of donor/acceptor-gating ion transfer and water activity differ for the $H_3O^+$/ $Na^+$ system and the $OH^-$/$ClO_4^-$ system, in both cases the two opposing modes of supporting electrolyte non-innocence cancel out. The ability to independently measure the ionic strength dependence of electrolyte proton activity and I-PCET kinetics suggests that the equal and opposite effect supporting electrolyte concentration has on proton donor/acceptor activity and pre-rate-limiting interfacial co-ion transfer is general to cations and anions, and that the relative strength of these effects can be qualitatively predicted based on the ions' solvation thermodynamics and coordinating ability.

In contrast to the stable rates observed in acidic and basic solutions, observed I-PCET rates decrease markedly in acetate buffered electrolytes at high ionic strengths. This observed decrease arises from the fact that the acceptor/donor couple responsible for setting bulk proton activity (acetic acid / acetate) is not the kinetically relevant couple for I-PCET. Thus, unlike in acidic solution, the sluggishness of displacing $Na^+$ from the EDL at high concentrations is not necessarily compensated by an increase in bulk proton activity. Indeed, it is observed that $pH_{eff}$ remains steady across the concentration range (**Figure 2**, green), suggesting that interactions between the acetate acid/acetate buffer and the supporting electrolyte are minimal (Error! Reference source not found., middle). On the other hand, as $H_3O^+$ remains the kinetically relevant proton donor, the need to displace a $Na^+$ ion from the surface remains. The slowing of $k_{app}$(pH,$m$) from 1 m to 17 m buffered $NaClO_4$ by 0.7 orders of magnitude (Error! Reference source not found.) at roughly constant $pH_{eff}$ is equivalent to the change in $k_{app}$(pH,$m$) that would be expected for a change in proton activity by 2 pH units at constant ionic strength, indicating $Na^+$ transfer between the interface and

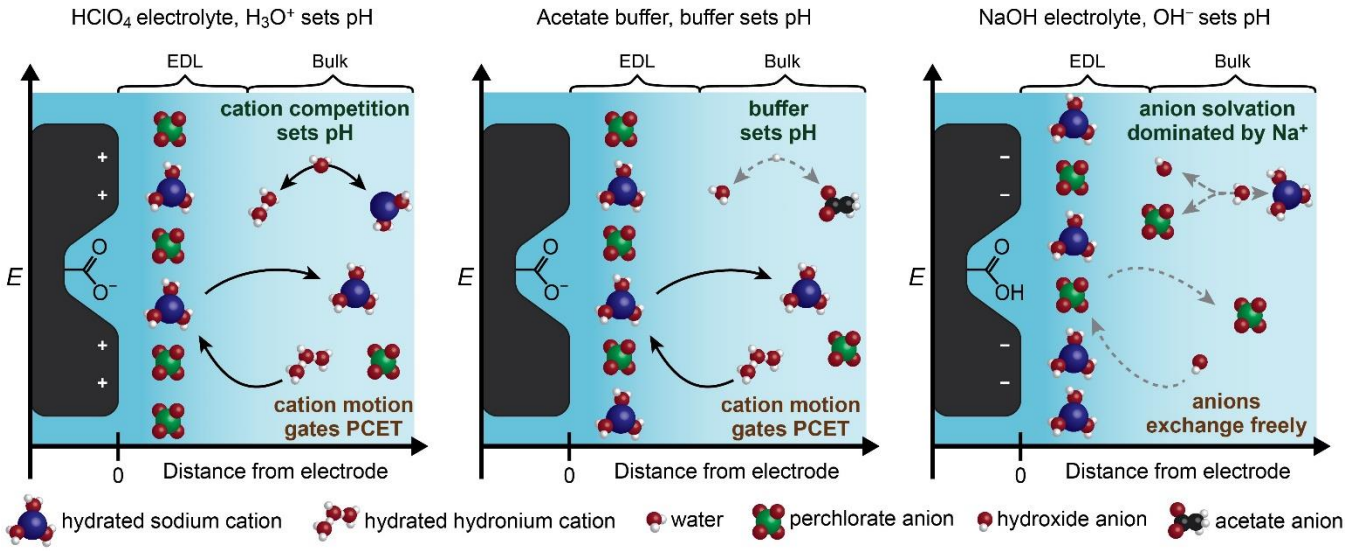


**Figure 8 | Ion interactions under acidic, buffered, and alkaline conditions. Left)** For acidic electrolytes, competition for solvation and ion repulsion increases $H_3O^+$ activity and inhibits $Na^+$ transfer to the bulk. These effects are equal and opposite, resulting in I-PCET rates that are molality independent. **Center)** For acetate buffered electrolytes, proton activity is kept constant by the buffer but $Na^+$ transfer to the bulk is still inhibited as molality increases, slowing I-PCET rates. **Right)** For alkaline electrolytes, competition and repulsion between $OH^-$ and $ClO_4^-$ result in minimal changes in $OH^-$ activity and $ClO_4^-$ transfer to the bulk, yielding no net change in I-PCET rates with ionic strength.

electrolyte gates I-PCET as long as $H_3O^+$ is the kinetically active I-PCET proton donor. The ability to independently measure $E_{RHE}$ and $k_{app}$(pH,$m$), and the differing molality dependence of each in the $HClO_4$ and acetate-buffered electrolytes, indicates that even when $pH_{eff}$ shifts with $Na^+_{bulk}$ activity, a conserved $Na^+_{bulk}$-activity-dependent interfacial ion transfer reaction controls I-PCET rate.

# Conclusion

In this study we leverage the molecular precision of graphite conjugated carboxylate electrode active sites to quantify how supporting electrolyte concentration controls the thermodynamics and kinetics of interfacial proton coupled electron transfer. Data collected from 1 molal to 17 molal aqueous $NaClO_4$ electrolytes for highly acidic, highly alkaline and mid-pH buffered electrolytes afford wide-ranging insight into these effects. We observed an effective pH decrease of nearly 2 units and no change in I-PCET rate with increasing electrolyte in acidic solution, no effective pH change and a decrease in I-PCET kinetics comparable to an effective pH increase of 2 units with increasing electrolyte in buffered solution, and no change in effective pH or I-PCET rate with increasing electrolyte concentration in basic solution. We attribute the shift in proton activity of the highly acidic electrolytes to an increased competition for $H_3O^+$ solvation as $Na^+$ concentration increases, whereas an increase in $ClO_4^-$ concentration has minimal effects on the solvation of $OH^-$ or acetate anions. Similarly, we attribute the relative slowing of I-PCET in the $HClO_4$ and acetate buffered electrolytes to the need for $H_3O^+$, the kinetically active proton donor, to displace a $Na^+$ ion at the electrochemical interface before rate limiting proton transfer. In basic electrolytes $ClO_4^-$ that must transfer to accommodate a $OH^-$ proton acceptor at the interface; however, this transfer is minimally inhibited at high concentrations. The observed effects of stable rate in acid and base and a rate decrease in buffered solutions can thus be understood as the composite of the aforementioned bulk and interfacial effects. These kinetic data strongly support a multistep mechanism for I-PCET in which an interfacial ion transfer reaction gates the formation of the PCET pre-association complex. Based on this mechanistic model, we introduce rate equations for I-PCET that incorporate bulk concentration dependent ion-activity dependencies to account for pre-rate-limiting interfacial ion transfer.

The mechanistic model presented above illustrates that supporting electrolyte ions play a critical role in interfacial proton-coupled electron transfer reactivity despite not being produced or consumed in I-PCET reactions. These ions unable to accept or donate protons themselves are not innocent in I-PCET reactivity and strongly influence solution proton activity and interfacial ion transfer. Our findings highlight that, although at interfaces proton and electron must transfer in a concerted step, a complete I-PCET reaction cannot simply be framed as a single elementary step, but as the series of five steps shown in **Figure 7**. To properly model I-PCET reactions, all five reactions, including the influence of supporting electrolyte and the movement of ions within the electrode/electrolyte boundary layer must be considered. The observed effect may only become apparent at high bulk ionic strength, however even at relatively dilute electrolytes where the interface may not be super-saturated, interfacial supporting electrolyte ions still exceed the bulk and so must move to accommodate the approach of ionic reactants to the electrode interface to form the hydrogen bonded pre-association complex. Understanding the role played by concentrated electrolyte solutions introduces new design principles for electrocatalytic systems and lends mechanistic insight into the preferential properties of highly concentrated media for electrochemical applications. For instance, concentrated electrolytes can be leveraged to promote the movement of neutral molecules across interfaces and on-electrode proton-free reactions such as the of C-C coupling to form multicarbon products in carbon dioxide reduction.[57] Moreover, buffered concentrated electrolytes can maintain optimal solution pH for reactants while slowing parasitic I-PCET side reactions. Finally, our results indicate that concentrated $HClO_4$ electrolytes allow modulation of effective solution pH without promoting parasitic I-PCET. This

observation, invoked in tandem with an interfacial pH swing assisted by the high concentration of solute,[68] shed light on the paradoxical slowing of hydrogen evolution rates observed in water-in-salt electrolytes as measured pH decreases.[13,22,46] In these ways electrolyte concentration and identity present a rational highly adjustable design parameter for developing the electrochemical devices essential for the clean energy transition.

## Acknowledgements

We gratefully acknowledge support from the Phase 1 Centers for Chemical Innovation Program in the U.S. National Science Foundation Division of Chemistry under Grant CHE-2221599.

# References


(1) Warburton, R. E.; Soudackov, A. V.; Hammes-Schiffer, S. Theoretical Modeling of Electrochemical Proton-Coupled Electron Transfer. *Chem. Rev.* **2022**, *122* (12), 10599–10650. https://doi.org/10.1021/acs.chemrev.1c00929.

(2) Pourbaix, M. *Atlas of Electrochemical Equilibria in Aqueous Solutions*; National Assoc. of Corrosion Engineers: Houston, Tex, 1974.

(3) Bard, A. J.; Faulkner, Larry R. *Electrochemical Methods: Fundamentals and Applications, Second Edition*; John Wiley & Sons, Inc., 2001.

(4) Mayer, J. M. Bonds over Electrons: Proton Coupled Electron Transfer at Solid–Solution Interfaces. *J. Am. Chem. Soc.* **2023**, *145* (13), 7050–7064. https://doi.org/10.1021/jacs.2c10212.

(5) Jung, O.; Jackson, M. N.; Bisbey, R. P.; Kogan, N. E.; Surendranath, Y. Innocent Buffers Reveal the Intrinsic pH- and Coverage-Dependent Kinetics of the Hydrogen Evolution Reaction on Noble Metals. *Joule* **2022**, *6* (2), 476–493. https://doi.org/10.1016/j.joule.2022.01.007.

(6) Dubouis, N.; Grimaud, A. The Hydrogen Evolution Reaction: From Material to Interfacial Descriptors. *Chem. Sci.* **2019**, *10* (40), 9165–9181. https://doi.org/10.1039/C9SC03831K.

(7) Reier, T.; Nong, H. N.; Teschner, D.; Schlögl, R.; Strasser, P. Electrocatalytic Oxygen Evolution Reaction in Acidic Environments – Reaction Mechanisms and Catalysts. *Advanced Energy Materials* **2017**, *7* (1), 1601275. https://doi.org/10.1002/aenm.201601275.

(8) Koper, M. T. M. Theory of Multiple Proton–Electron Transfer Reactions and Its Implications for Electrocatalysis. *Chem. Sci.* **2013**, *4* (7), 2710–2723. https://doi.org/10.1039/C3SC50205H.

(9) Schreier, M.; Yoon, Y.; Jackson, M. N.; Surendranath, Y. Competition between H and CO for Active Sites Governs Copper-Mediated Electrosynthesis of Hydrocarbon Fuels. *Angewandte Chemie International Edition* **2018**, *57* (32), 10221–10225. https://doi.org/10.1002/anie.201806051.

(10) Marcandalli, G.; Monteiro, M. C. O.; Goyal, A.; Koper, M. T. M. Electrolyte Effects on CO2 Electrochemical Reduction to CO. *Acc. Chem. Res.* **2022**, *55* (14), 1900–1911. https://doi.org/10.1021/acs.accounts.2c00080.

(11) Joo, J.; Uchida, T.; Cuesta, A.; Koper, M. T. M.; Osawa, M. Importance of Acid–Base Equilibrium in Electrocatalytic Oxidation of Formic Acid on Platinum. *J. Am. Chem. Soc.* **2013**, *135* (27), 9991–9994. https://doi.org/10.1021/ja403578s.

(12) Singh, C.; Paul, A. Physisorbed Hydroquinone on Activated Charcoal as a Supercapacitor: An Application of Proton-Coupled Electron Transfer. *J. Phys. Chem. C* **2015**, *119* (21), 11382–11390. https://doi.org/10.1021/acs.jpcc.5b01322.

(13) Bu, X.; Su, L.; Dou, Q.; Lei, S.; Yan, X. A Low-Cost "Water-in-Salt" Electrolyte for a 2.3 V High-Rate Carbon-Based Supercapacitor. *J. Mater. Chem. A* **2019**, *7* (13), 7541–7547. https://doi.org/10.1039/C9TA00154A.

(14) Cobb, S. J.; Ayres, Z. J.; Newton, M. E.; Macpherson, J. V. Deconvoluting Surface-Bound Quinone Proton Coupled Electron Transfer in Unbuffered Solutions: Toward a Universal Voltammetric pH Electrode. *J. Am. Chem. Soc.* **2019**, *141* (2), 1035–1044. https://doi.org/10.1021/jacs.8b11518.

(15) Ryu, J.; Wuttig, A.; Surendranath, Y. Quantification of Interfacial pH Variation at Molecular Length Scales Using a Concurrent Non-Faradaic Reaction. *Angewandte Chemie International Edition* **2018**, *57* (30), 9300–9304. https://doi.org/10.1002/anie.201802756.

(16) Wesley, T. S.; Román-Leshkov, Y.; Surendranath, Y. Spontaneous Electric Fields Play a Key Role in Thermochemical Catalysis at Metal−Liquid Interfaces. *ACS Cent. Sci.* **2021**, *7* (6), 1045–1055. https://doi.org/10.1021/acscentsci.1c00293.

(17) Howland, W. C.; Gerken, J. B.; Stahl, S. S.; Surendranath, Y. Thermal Hydroquinone Oxidation on Co/N-Doped Carbon Proceeds by a Band-Mediated Electrochemical Mechanism. *J. Am. Chem. Soc.* **2022**, *144* (25), 11253–11262. https://doi.org/10.1021/jacs.2c02746.
(18) Lodaya, K. M.; Tang, B. Y.; Bisbey, R. P.; Weng, S.; Westendorff, K. S.; Toh, W. L.; Ryu, J.; Román-Leshkov, Y.; Surendranath, Y. An Electrochemical Approach for Designing Thermochemical Bimetallic Nitrate Hydrogenation Catalysts. *Nat Catal* **2024**, *7* (3), 262–272. https://doi.org/10.1038/s41929-023-01094-0.
(19) Westendorff, K. S.; Hülsey, M. J.; Wesley, T. S.; Román-Leshkov, Y.; Surendranath, Y. Electrically Driven Proton Transfer Promotes Brønsted Acid Catalysis by Orders of Magnitude. *Science* **2024**. https://doi.org/10.1126/science.adk4902.
(20) Weng, S.; Toh, W. L.; Surendranath, Y. Weakly Coordinating Organic Cations Are Intrinsically Capable of Supporting CO2 Reduction Catalysis. *J. Am. Chem. Soc.* **2023**, *145* (30), 16787–16795. https://doi.org/10.1021/jacs.3c04769.
(21) Wuttig, A.; Yaguchi, M.; Motobayashi, K.; Osawa, M.; Surendranath, Y. Inhibited Proton Transfer Enhances Au-Catalyzed CO2-to-Fuels Selectivity. *Proc. Natl. Acad. Sci. U.S.A.* **2016**, *113* (32), E4585–E4593. https://doi.org/10.1073/pnas.1602984113.
(22) Suo, L.; Borodin, O.; Gao, T.; Olguin, M.; Ho, J.; Fan, X.; Luo, C.; Wang, C.; Xu, K. "Water-in-Salt" Electrolyte Enables High-Voltage Aqueous Lithium-Ion Chemistries. *Science* **2015**, *350* (6263), 938–943. https://doi.org/10.1126/science.aab1595.
(23) Qin, X.; Balbuena, P. B.; Shao, M. First-Principles Study on the Initial Oxidative Decompositions of Ethylene Carbonate on Layered Cathode Surfaces of Lithium-Ion Batteries. *J. Phys. Chem. C* **2019**, *123* (23), 14449–14458. https://doi.org/10.1021/acs.jpcc.9b02096.
(24) Choi, D.; Kang, J.; Park, J.; Han, B. First-Principles Study on Thermodynamic Stability of the Hybrid Interfacial Structure of LiMn 2 O 4 Cathode and Carbonate Electrolyte in Li-Ion Batteries. *Physical Chemistry Chemical Physics* **2018**, *20* (17), 11592–11597. https://doi.org/10.1039/C7CP08037A.
(25) Lundström, R.; Gogoi, N.; Melin, T.; Berg, E. J. Unveiling Reaction Pathways of Ethylene Carbonate and Vinylene Carbonate in Li-Ion Batteries. *J. Phys. Chem. C* **2024**. https://doi.org/10.1021/acs.jpcc.4c00927.
(26) Bard, A. J. Inner-Sphere Heterogeneous Electrode Reactions. Electrocatalysis and Photocatalysis: The Challenge. *J. Am. Chem. Soc.* **2010**, *132* (22), 7559–7567. https://doi.org/10.1021/ja101578m.
(27) Schmickler, W.; Santos, E. *Interfacial Electrochemistry*; Springer Science & Business Media, 2010.
(28) Sarabia, F.; Gomez Rodellar, C.; Roldan Cuenya, B.; Oener, S. Z. Exploring Dynamic Solvation Kinetics at Electrocatalyst Surfaces. *Nat Commun* **2024**, *15* (1), 8204. https://doi.org/10.1038/s41467-024-52499-9.
(29) Savéant, J. M.; Costentin, C. *Elements of Molecular and Biomolecular Electrochemistry: An Electrochemical Approach to Electron Transfer Chemistry*, Second edition.; Wiley: Hoboken, NJ, 2019.
(30) Costentin, C.; Robert, M.; Savéant, J.-M.; Teillout, A.-L. Concerted Proton-Coupled Electron Transfers in Aquo/Hydroxo/Oxo Metal Complexes: Electrochemistry of $[Os^{II}(Bpy)_2Py(OH_2)]^{2+}$ in Water. *Proc. Natl. Acad. Sci. U.S.A.* **2009**, *106* (29), 11829–11836. https://doi.org/10.1073/pnas.0905020106.
(31) Weinberg, D. R.; Gagliardi, C. J.; Hull, J. F.; Murphy, C. F.; Kent, C. A.; Westlake, B. C.; Paul, A.; Ess, D. H.; McCafferty, D. G.; Meyer, T. J. Proton-Coupled Electron Transfer. *Chem. Rev.* **2012**, *112* (7), 4016–4093. https://doi.org/10.1021/cr200177j.
(32) Costentin, C.; Robert, M.; Savéant, J.-M.; Teillout, A.-L. Concerted and Stepwise Proton-Coupled Electron Transfers in Aquo/Hydroxo Complex Couples in Water: Oxidative Electrochemistry of

[OsII(Bpy)2(Py)(OH2)]2+. *ChemPhysChem* **2009**, *10* (1), 191–198. https://doi.org/10.1002/cphc.200800361.
(33) Hammes-Schiffer, S.; Soudackov, A. V. Proton-Coupled Electron Transfer in Solution, Proteins, and Electrochemistry. *J. Phys. Chem. B* **2008**, *112* (45), 14108–14123. https://doi.org/10.1021/jp805876e.
(34) Su, L.; Chen, J.; Yang, F.; Li, P.; Jin, Y.; Luo, W.; Chen, S. Electric-Double-Layer Origin of the Kinetic pH Effect of Hydrogen Electrocatalysis Revealed by a Universal Hydroxide Adsorption-Dependent Inflection-Point Behavior. *J. Am. Chem. Soc.* **2023**, *145* (22), 12051–12058. https://doi.org/10.1021/jacs.3c01164.
(35) Jackson, M. N.; Surendranath, Y. Donor-Dependent Kinetics of Interfacial Proton-Coupled Electron Transfer. *J. Am. Chem. Soc.* **2016**, *138* (9), 3228–3234. https://doi.org/10.1021/jacs.6b00167.
(36) Jackson, M. N.; Jung, O.; Lamotte, H. C.; Surendranath, Y. Donor-Dependent Promotion of Interfacial Proton-Coupled Electron Transfer in Aqueous Electrocatalysis. *ACS Catal.* **2019**, *9* (4), 3737–3743. https://doi.org/10.1021/acscatal.9b00056.
(37) Kuo, D.-Y.; Lu, X.; Hu, B.; Abruña, H. D.; Suntivich, J. Rate and Mechanism of Electrochemical Formation of Surface-Bound Hydrogen on Pt(111) Single Crystals. *J. Phys. Chem. Lett.* **2022**, *13* (27), 6383–6390. https://doi.org/10.1021/acs.jpclett.2c01734.
(38) Lewis, N. B.; Bisbey, R. P.; Westendorff, K. S.; Soudackov, A. V.; Surendranath, Y. A Molecular-Level Mechanistic Framework for Interfacial Proton-Coupled Electron Transfer Kinetics. *Nat. Chem.* **2024**, *16* (3), 343–352. https://doi.org/10.1038/s41557-023-01400-0.
(39) Warburton, R. E.; Hutchison, P.; Jackson, M. N.; Pegis, M. L.; Surendranath, Y.; Hammes-Schiffer, S. Interfacial Field-Driven Proton-Coupled Electron Transfer at Graphite-Conjugated Organic Acids. *J. Am. Chem. Soc.* **2020**, *142* (49), 20855–20864. https://doi.org/10.1021/jacs.0c10632.
(40) Jackson, M. N.; Pegis, M. L.; Surendranath, Y. Graphite-Conjugated Acids Reveal a Molecular Framework for Proton-Coupled Electron Transfer at Electrode Surfaces. *ACS Cent. Sci.* **2019**, *5* (5), 831–841. https://doi.org/10.1021/acscentsci.9b00114.
(41) Jackson, M. N.; Surendranath, Y. Molecular Control of Heterogeneous Electrocatalysis through Graphite Conjugation. *Acc. Chem. Res.* **2019**, *52* (12), 3432–3441. https://doi.org/10.1021/acs.accounts.9b00439.
(42) Jackson, M. N.; Oh, S.; Kaminsky, C. J.; Chu, S. B.; Zhang, G.; Miller, J. T.; Surendranath, Y. Strong Electronic Coupling of Molecular Sites to Graphitic Electrodes via Pyrazine Conjugation. *J. Am. Chem. Soc.* **2018**, *140* (3), 1004–1010. https://doi.org/10.1021/jacs.7b10723.
(43) Eigen, M. Proton Transfer, Acid-Base Catalysis, and Enzymatic Hydrolysis. Part I: ELEMENTARY PROCESSES. *Angewandte Chemie International Edition in English* **1964**, *3* (1), 1–19. https://doi.org/10.1002/anie.196400011.
(44) Eigen, M. Kinetics of Proton Transfer Processes. *Discuss. Faraday Soc.* **1965**, *39*, 7. https://doi.org/10.1039/df9653900007.
(45) Reber, D.; Grissa, R.; Becker, M.; Kühnel, R.-S.; Battaglia, C. Anion Selection Criteria for Water-in-Salt Electrolytes. *Advanced Energy Materials* **2021**, *11* (5), 2002913. https://doi.org/10.1002/aenm.202002913.
(46) Zhao, Y.; Hu, X.; Stucky, G. D.; Boettcher, S. W. Thermodynamic, Kinetic, and Transport Contributions to Hydrogen Evolution Activity and Electrolyte-Stability Windows for Water-in-Salt Electrolytes. *J. Am. Chem. Soc.* **2024**. https://doi.org/10.1021/jacs.3c12980.
(47) Borodin, O.; Self, J.; Persson, K. A.; Wang, C.; Xu, K. Uncharted Waters: Super-Concentrated Electrolytes. *Joule* **2020**, *4* (1), 69–100. https://doi.org/10.1016/j.joule.2019.12.007.

(48) McEldrew, M.; Goodwin, Z. A. H.; Kornyshev, A. A.; Bazant, M. Z. Theory of the Double Layer in Water-in-Salt Electrolytes. *J. Phys. Chem. Lett.* **2018**, *9* (19), 5840–5846. https://doi.org/10.1021/acs.jpclett.8b02543.
(49) Suo, L.; Borodin, O.; Sun, W.; Fan, X.; Yang, C.; Wang, F.; Gao, T.; Ma, Z.; Schroeder, M.; von Cresce, A.; Russell, S. M.; Armand, M.; Angell, A.; Xu, K.; Wang, C. Advanced High-Voltage Aqueous Lithium-Ion Battery Enabled by "Water-in-Bisalt" Electrolyte. *Angewandte Chemie International Edition* **2016**, *55* (25), 7136–7141. https://doi.org/10.1002/anie.201602397.
(50) Suo, L.; Oh, D.; Lin, Y.; Zhuo, Z.; Borodin, O.; Gao, T.; Wang, F.; Kushima, A.; Wang, Z.; Kim, H.-C.; Qi, Y.; Yang, W.; Pan, F.; Li, J.; Xu, K.; Wang, C. How Solid-Electrolyte Interphase Forms in Aqueous Electrolytes. *J. Am. Chem. Soc.* **2017**, *139* (51), 18670–18680. https://doi.org/10.1021/jacs.7b10688.
(51) Han, J.; Mariani, A.; Passerini, S.; Varzi, A. A Perspective on the Role of Anions in Highly Concentrated Aqueous Electrolytes. *Energy Environ. Sci.* **2023**, *16* (4), 1480–1501. https://doi.org/10.1039/D2EE03682G.
(52) Liang, T.; Hou, R.; Dou, Q.; Zhang, H.; Yan, X. The Applications of Water-in-Salt Electrolytes in Electrochemical Energy Storage Devices. *Advanced Functional Materials* **2021**, *31* (3), 2006749. https://doi.org/10.1002/adfm.202006749.
(53) Dong, C.; Xu, F.; Chen, L.; Chen, Z.; Cao, Y. Design Strategies for High-Voltage Aqueous Batteries. *Small Structures* **2021**, *2* (7), 2100001. https://doi.org/10.1002/sstr.202100001.
(54) Lee, M. H.; Kim, S. J.; Chang, D.; Kim, J.; Moon, S.; Oh, K.; Park, K.-Y.; Seong, W. M.; Park, H.; Kwon, G.; Lee, B.; Kang, K. Toward a Low-Cost High-Voltage Sodium Aqueous Rechargeable Battery. *Materials Today* **2019**, *29*, 26–36. https://doi.org/10.1016/j.mattod.2019.02.004.
(55) Tomiyasu, H.; Shikata, H.; Takao, K.; Asanuma, N.; Taruta, S.; Park, Y.-Y. An Aqueous Electrolyte of the Widest Potential Window and Its Superior Capability for Capacitors. *Sci Rep* **2017**, *7* (1), 45048. https://doi.org/10.1038/srep45048.
(56) Sakamoto, R.; Yamashita, M.; Nakamoto, K.; Zhou, Y.; Yoshimoto, N.; Fujii, K.; Yamaguchi, T.; Kitajou, A.; Okada, S. Local Structure of a Highly Concentrated NaClO 4 Aqueous Solution-Type Electrolyte for Sodium Ion Batteries. *Physical Chemistry Chemical Physics* **2020**, *22* (45), 26452–26458. https://doi.org/10.1039/D0CP04376A.
(57) Zhang, H.; Gao, J.; Raciti, D.; Hall, A. S. Promoting Cu-Catalysed CO2 Electroreduction to Multicarbon Products by Tuning the Activity of H2O. *Nat Catal* **2023**, *6* (9), 807–817. https://doi.org/10.1038/s41929-023-01010-6.
(58) Degoulange, D.; Dubouis, N.; Grimaud, A. Toward the Understanding of Water-in-Salt Electrolytes: Individual Ion Activities and Liquid Junction Potentials in Highly Concentrated Aqueous Solutions. *The Journal of Chemical Physics* **2021**, *155* (6), 064701. https://doi.org/10.1063/5.0058506.
(59) Toner, J. D.; Catling, D. C. Water Activities of NaClO4, Ca(ClO4)2, and Mg(ClO4)2 Brines from Experimental Heat Capacities: Water Activity >0.6 below 200K. *Geochimica et Cosmochimica Acta* **2016**, *181*, 164–174. https://doi.org/10.1016/j.gca.2016.03.005.
(60) Marcus, Y. The Thermodynamics of Solvation of Ions. Part 2.—The Enthalpy of Hydration at 298.15 K. *J. Chem. Soc., Faraday Trans. 1* **1987**, *83* (2), 339. https://doi.org/10.1039/f19878300339.
(61) Laviron, E. General Expression of the Linear Potential Sweep Voltammogram in the Case of Diffusionless Electrochemical Systems. *Journal of Electroanalytical Chemistry and Interfacial Electrochemistry* **1979**, *101* (1), 19–28. https://doi.org/10.1016/S0022-0728(79)80075-3.
(62) Garlyyev, B.; Xue, S.; Watzele, S.; Scieszka, D.; Bandarenka, A. S. Influence of the Nature of the Alkali Metal Cations on the Electrical Double-Layer Capacitance of Model Pt(111) and Au(111) Electrodes. *J. Phys. Chem. Lett.* **2018**, *9* (8), 1927–1930. https://doi.org/10.1021/acs.jpclett.8b00610.

(63) Xue, S.; Garlyyev, B.; Auer, A.; Kunze-Liebhäuser, J.; Bandarenka, A. S. How the Nature of the Alkali Metal Cations Influences the Double-Layer Capacitance of Cu, Au, and Pt Single-Crystal Electrodes. *J. Phys. Chem. C* **2020**, *124* (23), 12442–12447. https://doi.org/10.1021/acs.jpcc.0c01715.
(64) Morales, J. W.; Galleguillos, H. R.; Hernández-Luis, F.; Rodríguez-Raposo, R. Activity Coefficients of NaClO4 in Aqueous Solution. *J. Chem. Eng. Data* **2011**, *56* (8), 3449–3453. https://doi.org/10.1021/je2005006.
(65) Sun, L.; Liang, X.; Solms, N. von; Kontogeorgis, G. M. Analysis of Some Electrolyte Models Including Their Ability to Predict the Activity Coefficients of Individual Ions. *Ind. Eng. Chem. Res.* **2020**, *59* (25), 11790–11809. https://doi.org/10.1021/acs.iecr.0c00980.
(66) Saravi, S. H.; Panagiotopoulos, A. Z. Individual Ion Activity Coefficients in Aqueous Electrolytes from Explicit-Water Molecular Dynamics Simulations. *J. Phys. Chem. B* **2021**, *125* (30), 8511–8521. https://doi.org/10.1021/acs.jpcb.1c04019.
(67) Valiskó, M.; Boda, D. Unraveling the Behavior of the Individual Ionic Activity Coefficients on the Basis of the Balance of Ion–Ion and Ion–Water Interactions. *J. Phys. Chem. B* **2015**, *119* (4), 1546–1557. https://doi.org/10.1021/jp509445k.
(68) Sauvé, E. R.; Tang, B. Y.; Razdan, N. K.; Toh, W. L.; Weng, S.; Surendranath, Y. Open Circuit Potential Decay Transients Quantify Interfacial pH Swings during High Current Density Hydrogen Electrocatalysis. *Joule* **2024**. https://doi.org/10.1016/j.joule.2024.01.004.